

Official Certificate

Julian Colorado

of

Pontificia Universidad Javeriana Bogota, Colombia

attended the

ICINCO 2019

16th International Conference on Informatics in
Control, Automation and Robotics

held in Prague - Czech Republic, July 29 - 31, 2019

and presented a paper entitled:

*Aerial Monitoring of Rice Crop Variables using an
UAV Robotic System*

as a conference speaker.

On behalf of the Organizing Committee,



Oleg Guskov
ICINCO Program Chair

Aerial Monitoring of Rice Crop Variables using an UAV Robotic System

C. Devia¹, J. Rojas^{1,3}, E. Petro², C. Martinez¹, I. Mondragon¹, D. Patino¹, C. Rebolledo^{2,3}
and J. Colorado¹

¹*School of Engineering, Pontificia Universidad Javeriana, Bogota, Colombia*

²*The International Center for Tropical Agriculture -CIAT, Agrodiversity, Palmira, Colombia*

³*CIRAD, AGAP-Pam, Montpellier, France*

Keywords: UAV, Precision Agriculture, Image Processing, Vegetative Indices, Multispectral Imagery, Machine Learning.

Abstract: This paper presents the integration of an UAV for the autonomous monitoring of rice crops. The system integrates image processing and machine learning algorithms to analyze multispectral aerial imagery. Our approach calculates 8 vegetation indices from the images at each stage of rice growth: vegetative, reproductive and ripening. Multivariable regressions and artificial neural networks have been implemented to model the relationship of these vegetation indices against two crop variables: biomass accumulation and leaf nitrogen concentration. Comprehensive experimental tests have been conducted to validate the setup. The results indicate that our system is capable of estimating biomass and nitrogen with an average correlation of 80% and 78% respectively.

1 INTRODUCTION

The use of Unmanned Aerial Vehicles (UAV) in the solution of agriculture-related problems spans a wide range of operations such as crop variable measurement (Gevaert et al., 2015), (Gago et al., 2015) fruit detection (Carrijo et al., 2017), crop plot detection (Hongli et al., 2017), crop yield improvement (Arroyo et al., 2017) and crop mapping (Guo et al., 2012), (Khanna et al., 2015). In (Dongyan Zhang, Xin-gen Zhou, Jian Zhang, Linsheng Huang and Zhao, 2017) the sheath blight fungus disease of rice was detected using a Phantom 2 UAV coupled with a high-resolution RGB multispectral camera (Micasense). Pix4D software was used to generate 2D and 3D geo-referenced maps and to compute different vegetation indices. In (Yong et al., 2016), (Lu et al., 2015), UAVs were used for nitrogen estimation and chlorophyll quantification (Uto et al., 2013) using hyperspectral sensors.

Multispectral images have been used in plant analysis for some time now (Naito et al., 2017). Initially, few vegetation indices were commonly used, mainly the Normalized Difference Vegetation Index (NDVI) for estimating above ground biomass. However, due to the presence of external factors such as water, soil backgrounds and the difference of the crop at each stage of growth, different vegetative indices were in-

troduced, such as the Soil-Adjusted Vegetation Index (SAVI), the Modified SAVI (MSAVI), the Modified Chlorophyll Absorption Ratio Index (MCARI) and the Modified Triangular Vegetation Index (MTVI), among others (Gnyp et al., 2014).

The development of an UAV-based crop monitoring system involves multiple challenges. In hardware terms the UAV requires sufficient autonomy to cover the crop area, also adequate on-board store capacity for high-resolution data, as well as low-weight sensors. The integration of the native UAV hardware with external sensors requires a significant interplay between hardware and software in order to guarantee data reliability, online processing and simple end-user experience. In previous work (Devia et al., 2019), we tackled these challenges by developing an autonomous UAV robotic system to monitor biomass dynamics based on NIR information. In this paper, we present a preliminary approach to also monitor leaf nitrogen concentration during the three main stages of plant growth: vegetative, reproductive and ripening. Our goal is to estimate biomass dynamics and nitrogen variations by calculating several vegetation indices from multispectral data. To this purpose, we present the robotic system architecture detailed in Figure 1. Two UAVs have been setup with both NIR and thermal cameras (upcoming work is oriented towards cooperative-UAV monitoring). For instance,

each robot captures a dataset of images independently and the processing is done in a PC base-station.

2 METHODS

2.1 UAV Robotic System

As mentioned, two UAVs were integrated: The ASCTEC Pelican¹ and the DJI Phantom². Also, the following equipment was used:

- ASCTEC Pelican:
 - ASCTEC autopilot.
 - Mastermind board for image processing and data acquisition.
 - Tetracam ADC-Lite multispectral camera: this camera captures visible light wavelengths longer than 520nm and near-infrared (NIR) wavelengths up to 920nm. The multispectral camera is located in the bottom of the drone and aligned with the center of mass.
- DJI Phantom:
 - DJI autopilot.
 - Parrot Sequoia multispectral camera³: his camera comes with 4 different sensor to capture image in different wavelengths: red, green, NIR and Red-Edge.
 - Flir duo R thermal camera⁴ with 640×512 in resolution with 32°C field of view. It incorporates a radiometric sensor operating at sampling frequency of 30Hz and capable of sensing the crop temperature between -20°C and 50°C with a resolution of $\pm 5^{\circ}\text{C}$.

The standard GPS waypoint navigation for both drones comes with a graphical user interface -GUI that allows for autonomous take-off, waypoint trajectory following and landing. In this work, the flight planning was enhanced with an additional module created for the image capturing planning process. This new module creates a GPS grid with the positions where the images must be taken in order to ensure appropriate image resolution, crop plot coverage and sufficient overlapping of images for ensuring reliable data-mapping of the crop. In this sense, our photo planner algorithm uses geometric parameters of the

NIR/thermal camera and the crop plot area to generate the cartesian points.

The required UAV altitude is also estimated in the photo planning algorithm. This is done by using the camera's field of view in each axis and the desired image resolution. Figure 2 presents experimental results regarding aerial crop coverage and geo-mapping of crop plots by applying classical image mosaicing techniques. The aforementioned methods were presented in previous works reported in (Rojas et al., 2017), (Jose et al., 2016), and (Rojas et al., 2018).

2.2 Crop Variable Estimation

This section addresses the challenges associated with NIR and thermal image processing to properly compute Vegetative Indices (VI). It mainly consists in three different stages:

1. Image processing: By taking raw images from the NIR camera, the system determines the crop area (plots) that are suitable for VI analysis. In this process we apply perspective corrections to the images (using drone's IMU information) and filtering strategies to remove the background and noise. Finally, NIR image segmentation is applied to extract the crop plot (parcel) of interest, as detailed by Figure 3(a).
2. Vegetation index computation: VI are well-known formulas that use the reflectance of the plants in different wavelengths to provide information about the health state of the plant. Table 1 details the VI used in this work and their corresponding formulas.
3. Machine Learning: Once the vegetative indices are computed, we applied Multivariable Regression models (MR) to calculate the accumulated biomass. Only polynomial models were considered using the vegetative indices as the independent variables. Furthermore, we also used Artificial Neural Networks (ANN) to estimate leaf nitrogen concentration by training our system during the three main stage of rice growth: vegetative, reproductive and ripening. Both MR and ANN models required a ground-truth dataset for training. In this sense, biomass and nitrogen were directly measured from the rice crop by following the traditional sampling method. For biomass, 1 linear meter of plants were cut from the ground, as detailed by Figure 3(b). Plants were sampled and weighted, then put in the oven at 65 degrees Celsius for 4 days or until a constant weight was reached. For nitrogen, we used a SPAD sensor (Soil-Plant Analyses Development) to directly measure leaf nitrogen.

¹<http://www.asctec.de/en/uav-uas-drones-rpas-roav/asctec-pelican/>

²<https://www.dji.com/phantom-4>

³<https://www.parrot.com>

⁴<https://www.flir.com/products/duo/>

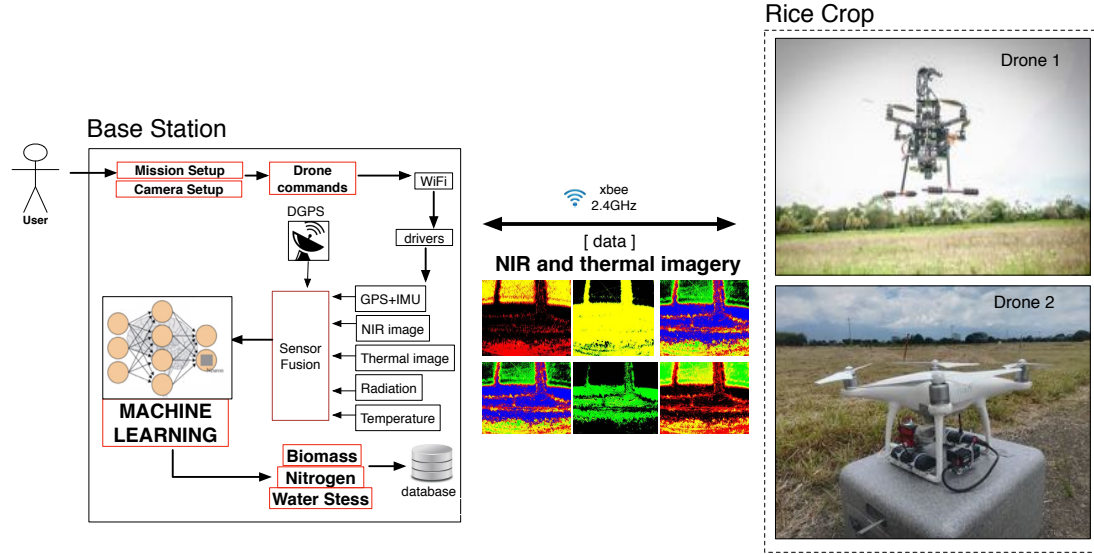


Figure 1: Multi-UAV robotic system architecture for crop monitoring.

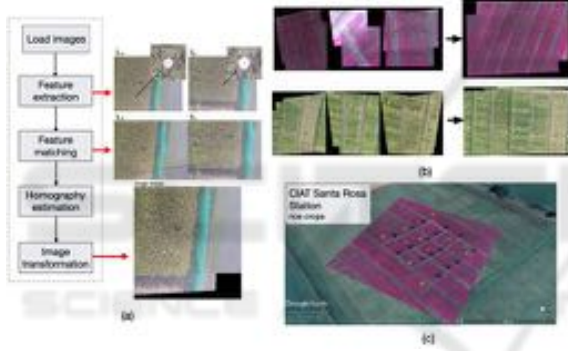


Figure 2: (a) image mosaicing flow diagram: SURF and ORB algorithms were implemented for feature extraction. The FLANN Fast (Library for Approximate Nearest Neighbors) algorithm was used for matching, whereas RANSAC (Random Sample Consensus) algorithm was used to create the homography for coordinate frame transformations. (b) Geo-referenced mosaicing results of applying the steps from (a) to both NIR and RGB images. (c) resulting NIR digital map of the crop and the trajectory followed by the drone.

3 EXPERIMENTAL RESULTS

Experiments were carried out during 2017 and 2018 in the rice farms of the Center of International Agriculture -CIAT, located in the Department of Meta, Colombia: latitude $4^{\circ}1'37.85''N$ with Longitude $73^{\circ}28'28.65''W$. Figure 4 shows experimental results for several weeks of in-field testing. Both MR and ANN methods have been used for the estimation of the crop variables based on NIR imagery. On average, the former, denoted as *Estimation 1*,

Table 1: NIR Vegetation Indices used (ρ_f denotes the reflectance of the for the frequency f) (Gnyp et al., 2014).

Name	Equation
Normalized Difference Vegetation Index -NDVI	$\frac{\rho_{780} - \rho_{670}}{\rho_{780} + \rho_{670}}$
Green Normalized Difference Vegetation Index -GNDVI	$\frac{\rho_{780} - \rho_{500}}{\rho_{780} + \rho_{500}}$
Soil-Adjusted Vegetation Index -SAVI	$(1 + L) \left(\frac{\rho_{800} - \rho_{670}}{\rho_{800} + \rho_{670} + L} \right)$ with $L = 0.5$
Modified SAVI -MSAVI	$\frac{1}{2} \left(2\rho_{800} + 1 - \sqrt{(2\rho_{800} + 1)^2 - 8(\rho_{800} - \rho_{670})} \right)$
Corrected Transformed Vegetation Index -CTVI	$\frac{NDVI + 0.5}{ NDVI + 0.5 } \sqrt{ NDVI + 0.5 }$
Difference Vegetation Index -DVI	$\rho_{780} - \rho_{670}$

achieves more accurate estimation compared against the ground-truth value, denoted as *Measurement*. The results are consistent for the three stages evaluated: vegetative, reproductive and ripening. The left plots of Figure 4 show the biomass and nitrogen estimation values respectively. Abrupt variations of the signals (e.g. sampled image 225 in the horizontal axis) indicates a change of crop stage from vegetative to reproductive. In this sense, the time evolution window of both crop variables is about 3 months.

Using the VIs and the metadata of the corresponding images, the multilinear regression models

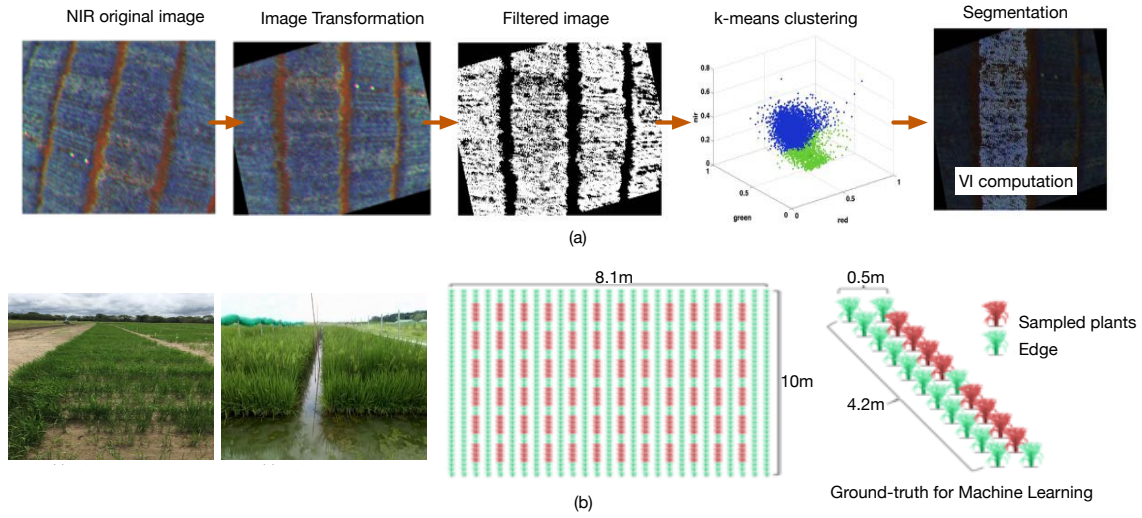


Figure 3: (a) Experimental results regarding NIR image pre-processing algorithms. Classical image clustering based on k-means has enabled to separate NIR pixels into two cluster: plant and no-plant. This allows the image background subtraction to properly extract the parcel of interest. (b) Ground-truth dataset for machine learning training.

Table 2: Numerical values for biomass and nitrogen/SPAD in vegetative stage directly measured from the crop (ground-truth values).

Plot/parcel	Repetition	Fresh weight [g]	Dry weight [g]	Water Content [g]	SPAD/nitrogen
13B1	1	656	118	82.01	47.70
38B4	1	394.00	76.00	80.71	45.30
63B1	1	450.00	88.00	80.44	34.27
88B4	1	814.00	100.00	87.71	41.23
13B5	2	792.00	136.00	82.83	44.37
38B8	2	420.00	76.00	81.90	46.53
63B5	2	646.00	120.00	81.42	43.07
88B8	2	550.00	104.00	81.09	40.30
13B9	3	626.00	126.00	79.87	36.63
38B12	3	656.00	110.00	83.23	44.10
63B9	3	428.00	76.00	82.24	38.13
88B12	3	540.00	108.00	80.00	43.63

were performed for every possible combination of vegetative indices. Strong linear dependencies were found between the VIs from Table 1 and the dynamics of biomass and nitrogen. For instance, linear multi-variable regressions of the form: $\beta_c \alpha_c + \beta_{SR} \alpha_{SR} + \beta_{NDVI} \alpha_{NDVI} + \beta_{GNDVI} \alpha_{GNDVI} + \beta_{CTVI} \alpha_{CTVI} + \beta_{SAVI} \alpha_{SAVI} + \beta_{DVI} \alpha_{DVI} + \beta_{MSAVI} \alpha_{MSAVI}$ were used to estimate both crop variables, computing the 7 VIs with a constant coefficient, where α_c , α_{SR} , α_{NDVI} , α_{GNDVI} , α_{CTVI} , α_{SAVI} , α_{DVI} and α_{MSAVI} take the value of 0 or 1. For each coefficient combination (VIs and the constant term), two images were taken randomly from each plot. This was done since not all the plots had the same number of photos, so if all the photos were used, the resulting regression could have some bias.

For each stage of the crop (vegetative, reproduc-

tive and ripening), we performed 20 flights, capturing around 2,000 images per stage, yielding a dataset of 6,000 images per trial. Overall, around 18,000 images were processed for the estimation of biomass and nitrogen. Both MR and ANN methods used a training set of NIR images accounting for the 60% of the entire database, whereas the remaining 40% for testing and validation. On the other hand, the correlations between estimated data and the ground-truth measurements are shown in the histograms depicted in the right plots of Figure 4. On average, our system is capable of estimating biomass and nitrogen with a correlation of 80% and 78% respectively⁵. Higher correlations above 80% were achieved during the first vegetative stage of the crop. During this stage, the

⁵The following video illustrates the steps performed during the experiments: <https://youtu.be/BTwD4GduXDo>

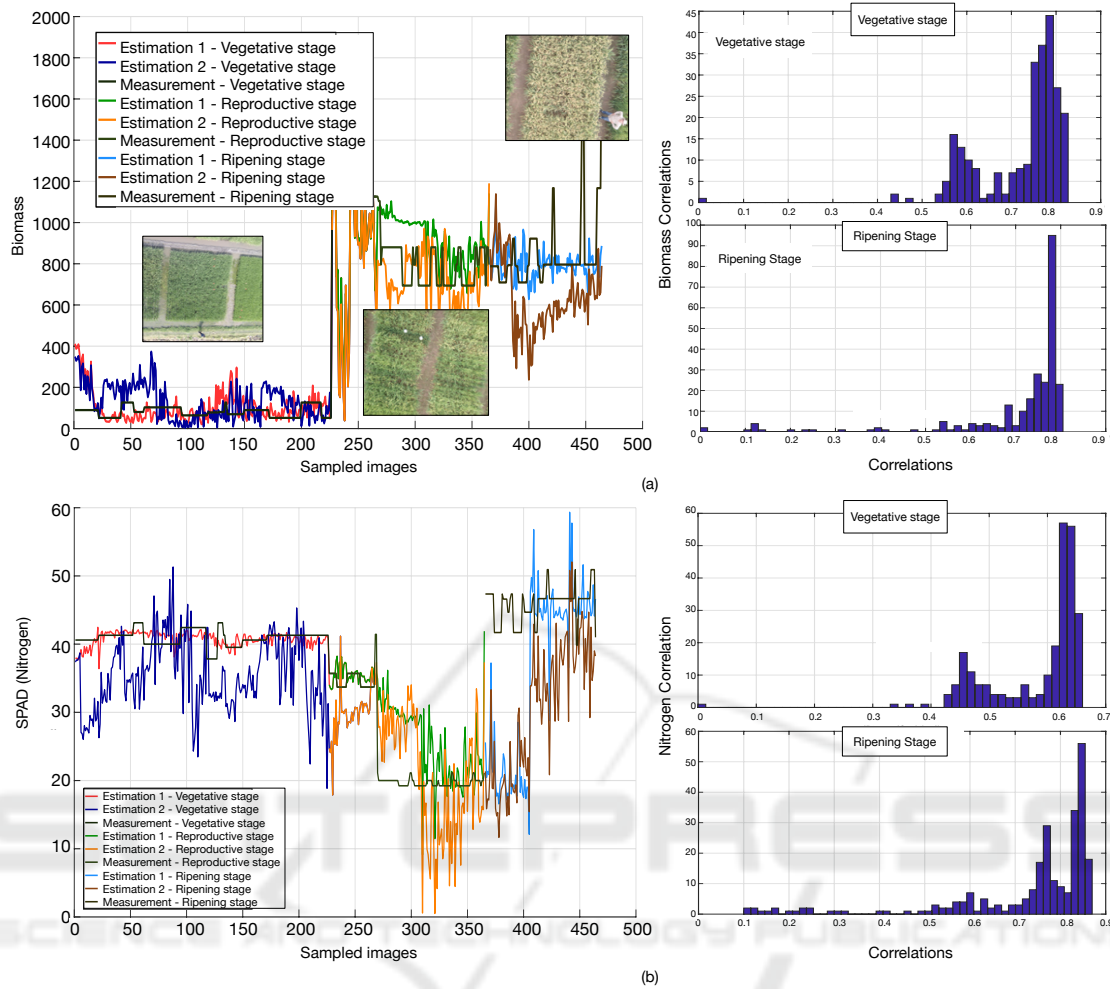


Figure 4: Experimental results (a) Biomass estimation (dry weight), (b) Nitrogen estimation. Left plots compare the estimated variables (labels Estimation 1 and 2) against the ground-truth labeled as Measurements. For nitrogen, this values is directly measured using a SPAD device. The time evolution window of both crop variables is about 3 months: vegetative, reproductive and ripening. Right plots contain the histogram information regarding the correlations achieved during the experiments.

green color of the plants is predominant, as observed by the inset in Figure 4(a). Therefore, our methods can be properly calibrated based on accurate VIs calculated from NIR image reflectances. Numerical values of the ground-truth measurements for the vegetative stage are considered in Table 2. The reproductive stage is more critical for our estimations algorithms since panicle formations yield yellow colors in the images. The merge of both green and yellow colors difficult the training, specially during the clustering phase where only two clusters are conformed: plants (green pixels) and no-plant (soil) cf. Figure 3(a). Larger fluctuations in biomass and nitrogen estimations occur in this crop stage, as observed in both Figure 4(a)(b) left plots. Lastly, in ripening stage, the yellow color becomes predominant, allowing a proper calibration and therefore accurate estimation of the

crop variables.

4 CONCLUSIONS

This paper presented the integration and deployment of an UAV system for rice crop monitoring. By using multivariable regressions and neural networks, our system was able to estimation biomass and nitrogen dynamics during the time evolution of the crop, concretely for three stages: vegetative, reproductive and ripening. From the specialized literature, we identified the set of vegetation indices that were sensible to biomass and nitrogen variations according to NIR image reflectance properties. We combined those indices to achieve the estimations of both values. A comprehensive field testing of the proposed system

enabled us to calculate correlations between the estimations and the in-field measurements of the crop variables. Since the vegetation indices tend to evolve linearly during the crop growth, we achieved accurate correlations using multivariable regressions; on average, correlations of 80% for biomass and 78% for nitrogen were achieved. Upcoming work is oriented towards improving the correlations by including more sophisticated image classification and clustering algorithms to consider several feature spaces for the NIR pixels. By now, our system is not reliable during the reproductive stage of the crop due to the mixed plant color in between yellow and green. Also, different genotypes of rice varieties are planted in the same plot area. In this sense, we also expect to improve on the estimation, since the biomass and nitrogen readings are highly dependent of the plant variety.

ACKNOWLEDGEMENTS

This work was funded in part by the OMICAS program: *Optimizaci3n Multiescala In-silico de Cultivos Agr3colas Sostenibles (Infraestructura y validaci3n en Arroz y Caña de Azúcar)*, sponsored within the Colombian Scientific Ecosystem by The WORLD BANK, COLCIENCIAS, ICETEX, the Colombian Ministry of Education and the Colombian Ministry of Industry and Tourism under GRANT ID: FP44842-217-2018. Also, by the research project entitled *Desarrollo de una herramienta para la agricultura de precision en los cultivos de arroz: sensado del estado de crecimiento y de nutrici3n de las plantas usando un dr3n autonomo*, under the COLCIENCIAS - GRANT ID 120371551916, CT167-2016 (FONDO NACIONAL DE FINANCIAMIENTO PARA LA CIENCIA, LA TECNOLOGIA Y LA INNOVACION -FRANCISCO JOSE DE CALDAS).

REFERENCES

- Arroyo, J. A., Gomez-Castaneda, C., Ruiz, E., de Cote, E. M., Gavi, F., and Sucar, L. E. (2017). Uav technology and machine learning techniques applied to the yield improvement in precision agriculture. In *2017 IEEE Mexican Humanitarian Technology Conference (MHTC)*, pages 137–143.
- Carrijo, G. L. A., Oliveira, D. E., de Assis, G. A., Carneiro, M. G., Guizilini, V. C., and Souza, J. R. (2017). Automatic detection of fruits in coffee crops from aerial images. In *2017 Latin American Robotics Symposium (LARS) and 2017 Brazilian Symposium on Robotics (SBR)*, pages 1–6.
- Devia, C. A., Rojas, J. P., Petro, E., Martinez, C., Mondragon, I. F., Patino, D., Rebolledo, M. C., and Colorado, J. (2019). High-throughput biomass estimation in rice crops using uav multispectral imagery. *Journal of Intelligent & Robotic Systems*.
- Dongyan Zhang, Xingen Zhou, Jian Zhang, Linsheng Huang, J. and Zhao (2017). Developing a small uav platform to detect sheath blight of rice. *IGRASS*, pages 7–10.
- Gago, J., Douthe, C., Coopman, R., Gallego, P., Ribas-Carbo, M., Flexas, J., Escalona, J., and Medrano, H. (2015). Uavs challenge to assess water stress for sustainable agriculture. *Agricultural Water Management*, 153:9 – 19.
- Gevaert, C. M., Suomalainen, J., Tang, J., and Kooistra, L. (2015). Generation of spectral 2013;temporal response surfaces by combining multispectral satellite and hyperspectral uav imagery for precision agriculture applications. *IEEE Journal of Selected Topics in Applied Earth Observations and Remote Sensing*, 8(6):3140–3146.
- Gnyp, M. L., Miao, Y., Yuan, F., Ustin, S. L., Yu, K., Yao, Y., Huang, S., and Bareth, G. (2014). Hyperspectral canopy sensing of paddy rice aboveground biomass at different growth stages. *Field Crops Research*, 155:42–55.
- Guo, T., Kujirai, T., and Watanabe, T. (2012). Mapping Crop Status From an Unmanned Aerial Vehicle for Precision Agriculture Applications. *ISPRS - International Archives of the Photogrammetry, Remote Sensing and Spatial Information Sciences*, XXXIX-B1(September):485–490.
- Hongli, L., Zhoumiqi, Y., Jinshui, Z., and Shuai, G. (2017). Highly efficient paddy classification using uav-based orthorectified image. In *2017 IEEE International Geoscience and Remote Sensing Symposium (IGARSS)*, pages 3230–3233.
- Jose, N., Ivan, M., Diego, P., and Julian, C. (2016). Multispectral mapping in agriculture: Terrain mosaic using an autonomous quadcopter UAV. In *2016 International Conference on Unmanned Aircraft Systems, ICUAS 2016*, pages 1351–1358.
- Khanna, R., Martin, M., Pfeifer, J., Liebisch, F., Walter, A., and Siegwart, R. (2015). Beyond Point Clouds - 3D Mapping and Field Parameter Measurements using UAVs. *IEEE 20th Conference on Emerging Technologies & Factory Automation*, pages 5–8.
- Lu, J., Miao, Y., Huang, Y., Shi, W., Hu, X., Wang, X., and Wan, J. (2015). Evaluating an unmanned aerial vehicle-based remote sensing system for estimation of rice nitrogen status. *2015 4th International Conference on Agro-Geoinformatics, Agro-Geoinformatics 2015*, pages 198–203.
- Naito, H., Ogawa, S., Valencia, M. O., Mohri, H., Urano, Y., Hosoi, F., Shimizu, Y., Chavez, A. L., Ishitani, M., Selvaraj, M. G., and Omasa, K. (2017). Estimating rice yield related traits and quantitative trait loci analysis under different nitrogen treatments using a simple tower-based field phenotyping system with modified single-lens reflex cameras. *ISPRS Journal of Photogrammetry and Remote Sensing*, 125(Supplement C):50 – 62.
- Rojas, J., Carlos, D., Petro, E., Martinez, C., Mondragon, I. F., Patino, D., Rebolledo, M., and Colorado, J.

- (2018). Aerial mapping of rice crops using mosaicing techniques for vegetative index monitoring. In *2018 International Conference on Unmanned Aircraft Systems (ICUAS)*, pages 846–855.
- Rojas, J., Martinez, C., Mondragon, I., and Colorado, J. (2017). Towards image mosaicking with aerial images for monitoring rice crops. In *Advances in Automation and Robotics Research in Latin America*, pages 279–296. Springer.
- Uto, K., Seki, H., Saito, G., and Kosugi, Y. (2013). Characterization of rice paddies by a UAV-mounted miniature hyperspectral sensor system. *IEEE Journal of Selected Topics in Applied Earth Observations and Remote Sensing*, 6(2):851–860.
- Yong, L., Tao, C., Yan, Z., Yongchao, T., Weixing, C., Xia, Y., Ni, W., Zheng, H., Zhou, X., Cheng, T., Yao, X., Tian, Y., Cao, W., and Zhu, Y. (2016). Comparative analysis of vegetation indices , non-parametric and physical retrieval methods for monitoring nitrogen in wheat using UAV-based multispectral imagery Yong Liu , Tao Cheng , Yan Zhu , Yongchao Tian , Weixing Cao , Xia Yao *, Ni Wang National En. *Ieee*, pages 7350–7353.

